JGR Oceans

RESEARCH ARTICLE
10.1029/2018JC014574

Special Section:
Recent Progresses in Oceanography and Air-Sea Interactions in Southeast Asian Archipelago

This article is a companion to Gordon et al. (2019), https://doi.org/10.1029/2018JC014502.

Unprecedented Response of Indonesian Throughflow to Anomalous Indo-Pacific Climatic Forcing in 2016

Kandaga Pujiana[1,2], Michael J. McPhaden[1], Arnold L. Gordon[3], and Asmi M. Napitu[3,4]

[1]NOAA Pacific Marine Environmental Laboratory, Seattle, WA, USA, [2]Faculty of Earth Sciences and Technology, Bandung Institute of Technology, Bandung, Indonesia, [3]Lamont-Doherty Earth Observatory, Columbia University, Palisades, NY, USA, [4]Ministry of Marine Affairs and Fisheries of Republic of Indonesia, Jakarta, Indonesia

Abstract The Indonesian Throughflow (ITF) transport in the upper layer of Makassar Strait was reduced by an unprecedented 25–40% during June to September 2016, the weakest northern summer ITF transport measured through 2004 to mid-2017. A negative Indian Ocean Dipole (IOD) event occurring through boreal summer and fall 2016 was the main driver for the reduced ITF transport. Elevated sea surface temperature and height off the southern coast of Sumatra and Java islands, attributed to the IOD event, suppressed the Pacific to Indian pressure gradient, resulting in a reduction in the ITF transport. Intensified Wyrtki jets, energetic westerly winds, and downwelling Kelvin waves associated with the strong IOD event contributed to the suppressed interocean pressure gradient. The influence from the 2016 La Niña event on the other hand was secondary. This study showcases the role of coupled ocean-atmosphere interactions in Indian Ocean in regulating an extreme interannual variation of the ITF in 2016, which is a unique event in the observational record.

Key Points:
- The Indonesian Throughflow in the upper layer of Makassar Strait in June–September 2016 was the weakest in boreal summer in the past decade
- The Pacific to Indian Ocean sea level pressure gradient in 2016 was primarily due to an unprecedented negative Indian Ocean Dipole event
- The unprecedented dipole event was thus responsible for the anomalous Indonesian Throughflow transport

Correspondence to:
K. Pujiana,
kandaga.pujiana@noaa.gov

Citation:
Pujiana, K., McPhaden, M. J., Gordon, A. L., & Napitu, A. (2019). Unprecedented response of Indonesian Throughflow to anomalous Indo-Pacific climatic forcing in 2016. *Journal of Geophysical Research: Oceans*, *124*, 3737–3754. https://doi.org/10.1029/2018JC014574

Received 15 SEP 2018
Accepted 11 FEB 2019
Accepted article online 1 MAY 2019
Published online 13 JUN 2019

1. Introduction

The Indonesian Throughflow (ITF) is part of the global thermohaline circulation that facilitates the transport of heat and fresh water from the Pacific to the Indian Ocean, through multiple straits in the Indonesian maritime continent, and hence modifies ocean heat and freshwater inventories as well as ocean-atmosphere exchanges on a broad range of time scales in the Indo-Pacific warm pool (Gordon, 1986; Gordon & Fine, 1996; Lee et al., 2002; Santoso et al., 2011). Moreover, changes in sea surface temperature (SST) over the warm pool where the ascending branch of the Walker Circulation lies may feedback to the atmosphere and subsequently modulate the climate system in the global tropics (Godfrey, 1996; Sprintall et al., 2014). Any shifts in the mean state and variability of oceanic and atmospheric processes in the Indo-Pacific region therefore affect the ITF and vice versa.

Trade winds over the western Pacific and Australian-Indonesian monsoon winds together maintain a pressure difference between the Pacific and Indian Ocean that regulates the mean and variability of the ITF (Wyrtki, 1987). Easterly driven upwelling off the southern coasts of Sumatra and Java lowers sea surface height (η) in the southeastern Indian Ocean and increases the interocean pressure head directed towards the Indian Ocean that consequently results in maximum ITF transport during the southeast monsoon in boreal summer, i.e. June to September (Figures 1b and 1d; Masumoto & Yamagata, 1996). The opposite holds during the northwest monsoon, December to March, when the ITF transport is at a minimum (Figures 1a and 1c; Gordon et al., 2012).

Since the large-scale pressure gradient is controlled by winds over the Pacific and Indian Ocean, the ITF responds to El Niño-Southern Oscillation (ENSO) and the Indian Ocean dipole (IOD). Numerical experiments and reanalysis data-based studies have suggested that the ITF is generally stronger during La Niña and during positive IOD events, while it becomes weaker during El Niño and during negative IOD events (Masumoto, 2002; Murtugudde et al., 1998; Potemra & Schneider, 2007). Sprintall and Revelard (2014), using indirect estimates of ITF transport through the ITF outflow passages in the Indonesian seas, arrived at a similar conclusion. Equatorial wave guides intersecting in the Indonesian Seas support transmission of changes occurring in the Pacific to the Indian Ocean and vice versa, impacting the pressure gradient between the two basins and subsequently ITF variations (Pujiana et al., 2013; Sprintall et al., 2000; Wijffels & Meyers, 2004; Yuan et al., 2013).

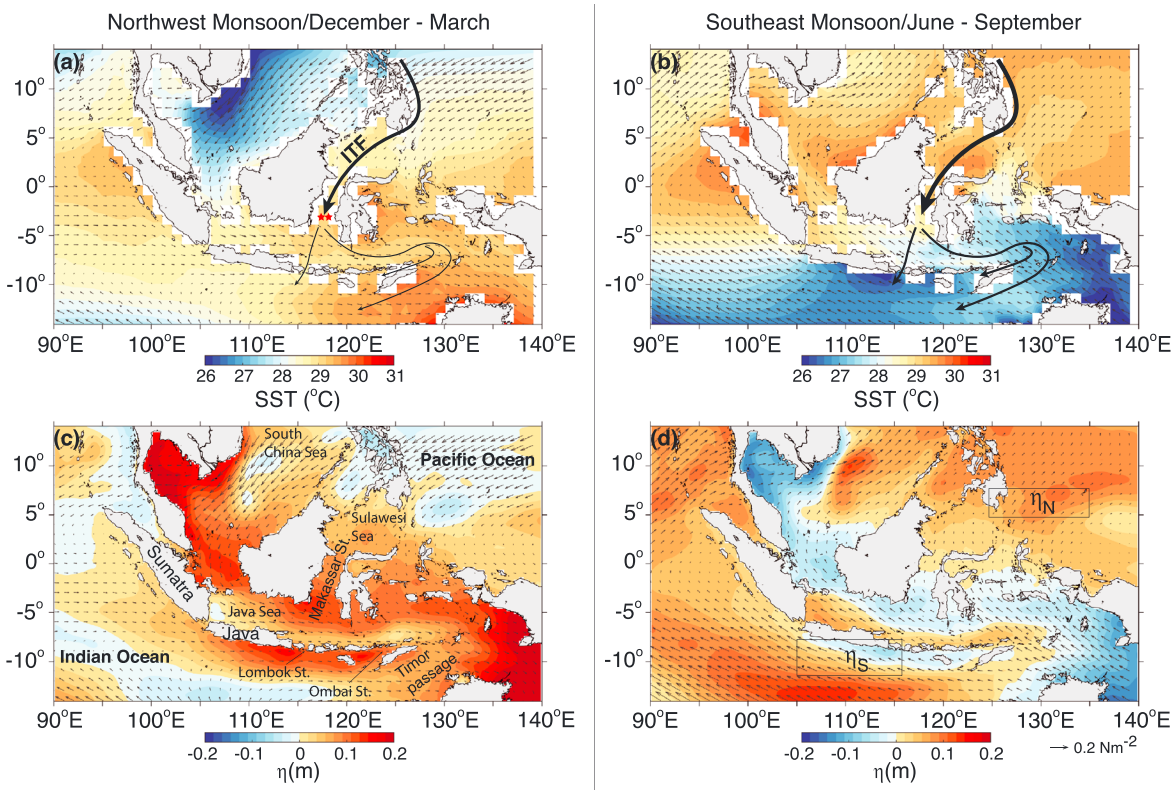

Figure 1. Seasonal averages of sea surface temperature (SST), sea surface height (η), and wind stress (τ) during two main Australian-Indonesian monsoons inferred from satellite-retrieved SST and observed between 2004 and 2017. (a) and (c), respectively, show SST and η during the northwest monsoon/December to March, while (b) and (d), respectively, demonstrate SST and η during the southeast monsoon/June to September. Arrows mark τ. Red stars in (a) indicate mooring sites in Makassar Strait. Thick arrows in (a) and (b) show simplified Indonesian Throughflow pathways in the Indonesian seas.

Marked changes in the Pacific and Indian Oceans, including those attributed to the ITF, have been observed over the recent decades. Associated with the recent hiatus in global surface warming (Kosaka & Xie, 2013), for example, the trade winds in the Pacific intensified (England et al., 2014), and upper ocean heat content substantially increased in the Indian Ocean through 2003–2012 (Nieves et al., 2015). Lee et al. (2015), using numerical experiments, suggested that increased trade wind-driven ITF heat transport was the cause of the heat gain in the Indian Ocean. Observations (Gordon et al., 2012; Sprintall & Revelard, 2014) and ocean reanalysis products (Dong & McPhaden, 2016) revealed strengthened ITF transport during this period, confirming the model results.

Similarly, model-based studies by Lim and Hendon (2017), Lu et al. (2017), and Mayer et al. (2018) revealed pronounced impacts of the Indian Ocean warming on the development of an extreme negative IOD and weak La Niña events during northern summer to fall 2016. Lu et al. (2017) posited that the long-term increasing trend in surface and subsurface temperatures in the Indian Ocean deepened the thermocline in the eastern basin, promoting strengthened thermocline feedback favorable for the development of the negative IOD event. They also suggested that the big 2015–16 El Niño event partly controlled the warming trend in the central Indian Ocean. Mayer et al. (2018) argued that decadal variation-induced anomalously warm Indian Ocean during 2015–2016 reduced the cross-basin pressure gradient and consequently the ITF, which in turn caused weaker than usual turbulent cooling into the atmosphere associated with the 2015–2016 El Niño and resulted in a weak La Niña in 2016. Lim and Hendon (2017) proposed that the weak 2016 La Niña may have eventuated from the 2015 El Niño that lasted until early spring 2016, maintaining strong westerlies in the western Pacific. They reasoned that without the negative IOD event-driven anomalous easterlies counteracting the prolonged El Niño-forced westerlies in the western Pacific, the weak 2016 La Niña would have been weaker.

Using direct ITF measurements over the course of 2004 to mid-2017 in Makassar Strait (Figure 1c), the ITF primary inflow passage in the Indonesian seas (Gordon et al., 1999, 2010), we aim to elucidate the unusual

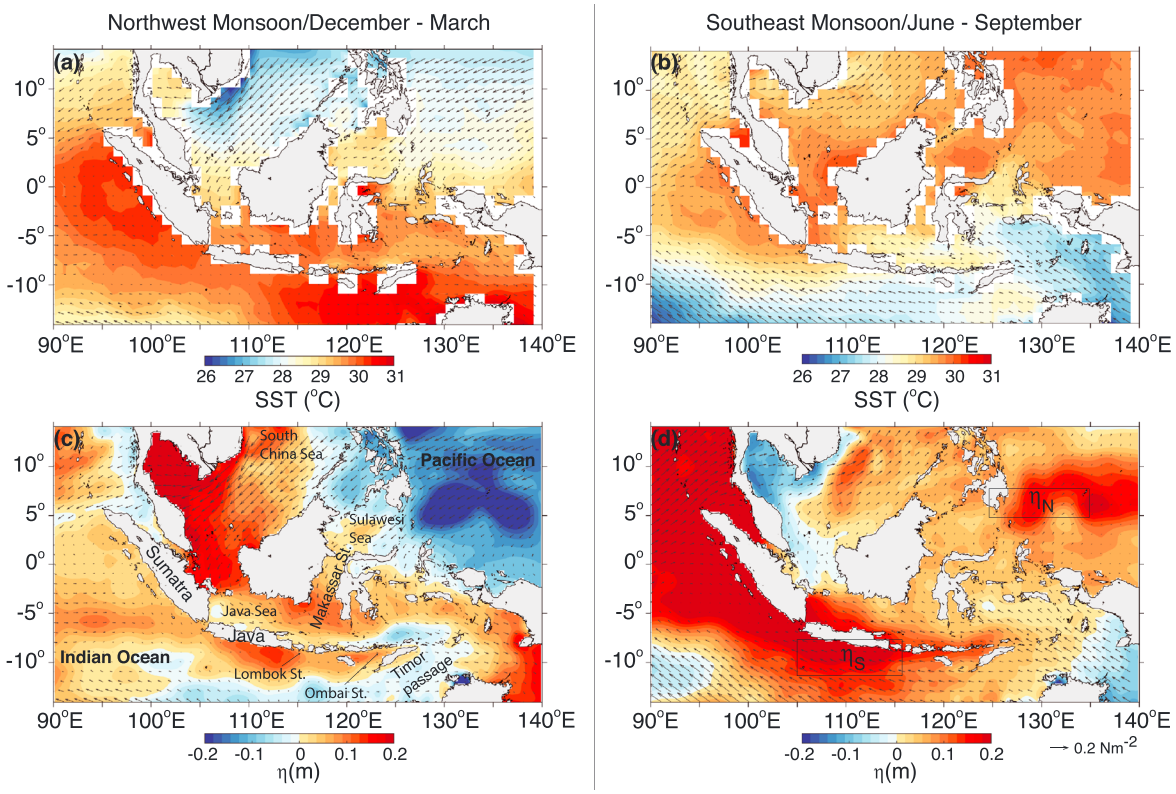

Figure 2. As in Figure 1 but for 2016.

ITF changes occurring primarily between June and September 2016, during which the ITF transport in the upper 300 m was greatly reduced compared to boreal summer ITF transports observed in previous years. Through the anomalous period, SST off the southern coasts of Java and Sumatra was warmed by about 2 °C, on average, partly resulting in an increase of η there by up to 0.4 m (Figures 2b and 2d). We will demonstrate how the anomalous ITF over boreal summer 2016 is linked to the strongest negative IOD event in the past decades. The negative IOD event was preceded by a big El Niño event through fall 2015 to early 2016, marked by substantially colder SST and depressed η over the western Pacific (Figures 2a and 2c).

The rest of this paper starts with section 2 describing data and methods. Section 3 discusses seasonal variations and anomalies of the ITF observed in Makassar Strait and the interocean pressure gradient and describes the relationships between ITF anomalies, pressure gradient anomalies, and ENSO/IOD. This is followed by assessments of the links between oceanic processes in the equatorial Indian Ocean, including those attributed to the negative IOD 2016, and the ITF in section 4. We conclude with a summary and discussion.

2. Data and Methods

2.1. Moored Data

Direct estimates of ITF transport used throughout this study were derived from velocity measurements at two subsurface moorings deployed at a 45-km-wide narrow constriction in Makassar Strait (Figure 1a). Each mooring was instrumented by a set of Acoustic Doppler Current Profilers (ADCPs) and current meters at selected depths, resolving along-strait (v) and across strait (u) velocities between 40 and 760 m. Near-surface velocities were excluded due to biases from side lobe reflections from the surface. The mooring on the western side of the strait was deployed during January 2004 to July 2011 and from August 2013 to July 2017, while the other mooring was operational over 2004–2006. Sampling rates varied from 1 to 2 hr.

Estimating the along-strait ITF transport consisted of three steps. First, the v profiles of the two moorings were laterally interpolated between the moorings and extrapolated to the strait side walls, resulting in the laterally and vertically gridded v data. Second, the cross-strait averaged v or along-strait transport per unit

depth was computed from the gridded v data. Third, the volume transport was approximated by a vertical integral of the transport per unit depth between two depth levels. Estimating transport between January 2007 to July 2011 and August 2013 to July 2017, through which only the western mooring was operational, was based on a high correlation between velocities observed from the two moorings observed during 2004–2006. The transport sign convention used throughout this paper is that negative values indicate transport into the Indian Ocean or southward transport and vice versa for positive values. Details on the Makassar Strait mooring configuration are documented in Gordon et al. (2008) and Gordon et al. (2010).

To help simplify the analysis, we divide the water column in Makassar Strait across which the ITF transport was observed into two layers, surface to 300 m (upper layer) and 300–760 m (lower layer). The water column partition used here is consistent with that applied by Gordon et al. (2019), in which the depth demarcating the two layers corresponds with the core depth of salinity minimum attributed to the North Pacific Intermediate Water observed in Makassar Strait (Ilahude & Gordon, 1996). We will hereafter, respectively, refer the layer between the surface and 300 m and 300 m and 760 m as the upper layer and the lower layer.

In addition to the Makassar mooring data, hourly surface wind stress (τ), and upper ocean velocities from a wind gauge and an ADCP deployed at a mooring at 0°, 80° E, part of the Research Moored Array for African-Asian-Australian Monsoon Analysis and Prediction (RAMA) (McPhaden et al., 2009) observed between 2004 and July 2017 were employed. Gridded velocities between the surface and 300 m at a 5-m interval were examined, with velocities near the surface linearly extrapolated from the ADCP velocities at 30 m. The interpolated velocities compare reasonably well with the current meter velocities at 10 m (Nagura & McPhaden, 2010a). Daily averages of data from the Makassar Strait and RAMA moorings are used for the analyses.

2.2. Satellite-Derived and Reanalysis Data

To provide insights into physical processes relevant with the ITF over the Indo-Pacific region, we examined gridded satellite-retrieved SST, τ, and η, with a horizontal and temporal resolution of 0.25° × 0.25° and daily, complementing the moored data. We made use the National Oceanic and Atmospheric Administration (NOAA) Optimum Interpolation SST product (Reynolds et al., 2007), near-real-time Institut Français de Recherche pour l'exploitation de la Mer wind stress product (Bentamy et al., 2002), and Archiving, Validation and Interpretation of Satellite Oceanographic data surface height product (Ducet et al., 2000) encompassing a period between 2004 and 2017. Upper ocean circulation in the Indo-Pacific basins was estimated using a reanalysis product from Ocean Surface Current Analysis Real Time, available as 5-day averages on a 1° × 1° grid (Bonjean & Lagerloef, 2002). As with the moored and other satellite-sourced data sets, the Ocean Surface Current Analysis Real Time data were interpolated to daily resolution.

As indicators of IOD and ENSO events, we employed the Dipole Mode Index (DMI) and NINO 3.4 index, respectively, a product of NOAA Earth System Research Laboratory. The weekly indices were interpolated to daily time series, matching the time resolution of the other data sets. Definitions of IOD and ENSO events applied here adopt the classifications made by Saji and Yamagata (2003) and L'Heureux et al. (2017), respectively.

3. Variability of the ITF Transport and Interocean Pressure Gradient

3.1. Mean Seasonal Cycle

Long-term ITF measurements in Makassar Strait, extending for about 11.5 years (Figure 3a), allow computation of mean seasonal cycle of ITF transport. Smoothed with a 61-day triangle filter and then averaged across different years, daily averages of total ITF transport in the upper 760 m in Makassar Strait clearly demonstrate a mean seasonal cycle exhibiting a maximum magnitude of −15.8 ± 1.7 Sv in August and a minimum magnitude of −8.9 ± 1.9 Sv in December (black curve in Figure 4a). In general, the ITF seasonal cycle is in agreement with that derived from shorter time series in Makassar Strait (Gordon et al., 2008; Susanto et al., 2012), inferred from the satellite-based proxy transport (Sprintall & Revelard, 2014) and estimated by model-based studies (Masumoto & Yamagata, 1996; Potemra & Lukas, 1999; Shinoda et al., 2012). Readers are referred to Gordon et al. (2019) for details of the seasonal cycle of ITF transport elucidated from the long-term measurements in Makassar Strait.

The seasonal cycle of ITF transport is related to the seasonal variation of the Pacific to Indian Ocean pressure gradient ($\delta\eta$), the difference between η over the western pacific (η_N) and η off the coast of Java (η_S; Figure 3d). Concurrent with the period of maximum ITF transport, largest $\delta\eta$ occurs in boreal summer (Figure 4b).

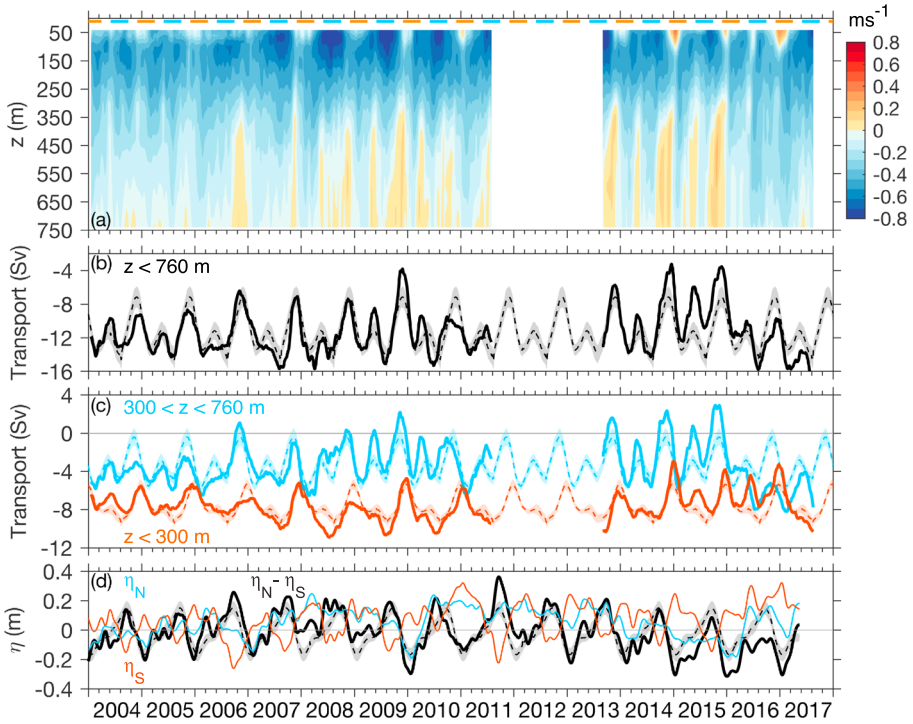

Figure 3. Filtered daily time series of (a) average v of the two moorings, (b) total transport in the upper 760 m, (c) total transport in the upper 300 m (upper layer, red) and between 300 and 760 m (lower layer, blue) in Makassar Strait, and (d) the interocean pressure gradient, $\delta\eta$, observed between January 2004 and July 2017. Negative values of transport indicate Indonesian Throughflow transport toward the Indian Ocean. Blue and red curves in (d), respectively, show η averaged over areas encompassing western Pacific (η_N) and that averaged over off the southern coast of Java (η_S) as indicated in Figure 1d. Color coded dashed lines and shaded curves, respectively, indicate mean seasonal cycle and its 95% bootstrap confidence limits. Orange and blue horizontal bars in (a), respectively, indicate northwest monsoon months (December–March) and southeast monsoon months (June–September). A 61-day triangle filter was employed to smooth the daily time series.

Minimum ITF transport during boreal winter coincides with the suppressed $\delta\eta$. Monsoon-driven fresh water input from the South China and Java Seas and equatorial wave dynamics in the Pacific and Indian Oceans together dictate the seasonal cycle of $\delta\eta$ (Gordon et al., 2012; Potemra & Lukas, 1999). The pressure gradient appears to control the bulk of seasonal variation of the ITF transport confined in the upper layer. Monthly averages of seasonal cycles of $\delta\eta$ and total transport in the upper layer show a significant correlation of -0.77 ($p < 0.01$; orange dots in Figure 4c). When the ITF transport is integrated in the upper 100 m, the correlation coefficient between its total transport and $\delta\eta$ increases to -0.81. Local along-strait τ generally is not important for seasonal variation of the ITF but is influential to drive subseasonal variations of the ITF in the upper layer of Makassar Strait (Pujiana et al., 2009). Note that the areas used to determine η_N and η_S are similar to those adopted in previous studies (Mayer et al., 2018; Shinoda et al., 2012).

The seasonal cycle of ITF transport, especially in the lower layer, exhibits secondary minima in May and November (Figures 3b, 3c, and 4a). Reduced ITF transport during monsoon transition months, April–May and October–November, has been attributed to intrusions of coastally trapped Kelvin waves propagating along the southern coasts of Sumatra and Java, originating in the equatorial Indian Ocean, into Makassar Strait (Pujiana et al., 2013; Sprintall et al., 2000). Annual upwelling Rossby waves, propagating from the eastern equatorial Pacific Ocean, may also contribute to reduce the interocean pressure gradient and hence the ITF during the monsoon transition periods (Potemra & Lukas, 1999). As a result, the correlation between $\delta\eta$ and transport in the upper 760 m is only -0.28 ($p > 0.01$) compared to the stronger correlation at shallower levels (Figure 4c).

3.2. Anomalies

Figure 3a illustrates the complexity of the vertical structure of ITF variability in Makassar Strait. The leading empirical orthogonal function (EOF) mode of seasonal anomalies of the average v of the two moorings,

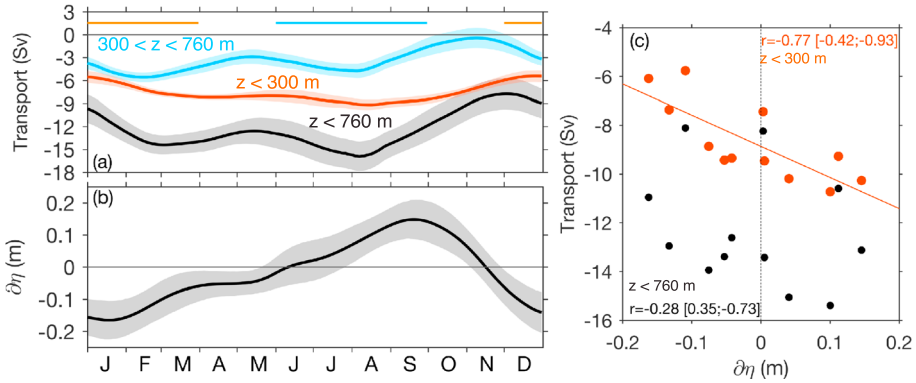

Figure 4. Mean seasonal cycle of (a) total Indonesian Throughflow transport in the upper 300 m (upper layer, red), between 300 and 760 m (lower layer, blue), and in the upper 760 m (black) observed in Makassar Strait and (b) $\delta\eta$ for January 2004 to July 2017 based on the filtered, daily time series in Figure 3. Negative values of transport indicate Indonesian Throughflow transport toward the Indian Ocean. Positive values of $\delta\eta$ denote higher η in the western Pacific than off Java. Color coded shaded curves indicate 95% bootstrap confidence limits. Orange and blue horizontal bars in (a), respectively, mark northwest monsoon months (December–March) and southeast monsoon months (June–September). (c) Scatter plots of monthly averages of the mean seasonal cycle of transport versus the mean seasonal cycle of $\delta\eta$ for total transport in the upper layer (orange) and in the upper 760 m (black) at zero lag. Values within the brackets indicate 95% confidence limits.

accounting for about 72% of the anomalies, reveals a vertical mode with a zero crossing between 250 and 300 m (Figure 5), supporting a two-layer system that we define here. Note that the anomalies were obtained by subtracting the mean seasonal cycle from the smoothed time series shown in Figures 3a–3c. The seasonal anomalies will be henceforth referred to as anomalies.

Peaks and troughs of the upper layer transport anomalies generally occurred in boreal winter and summer, respectively, with negative anomalies marking the transport during 2007–2011 and positive anomalies dominating the transport through 2004–2006 and 2014–2017 (red curve in Figure 6a). The positive transport anomalies were profound in the summers of 2004–2005, which coincided with negative anomalies of $\delta\eta$ and weak negative IOD events (Figures 6a and 7a–7c). Pronounced positive anomalies of ITF transport were also observed in the monsoon transition months of April–May and October–November through 2004–2006 (Figure 6a), marking penetrations of semiannual Kelvin waves from the Indian Ocean to Makassar Strait (Pujiana et al., 2009). The extended period of negative transport anomalies between 2007 and 2011 may reflect ITF response to strengthened trade winds in the Pacific (England et al., 2014), characterizing the surface warming hiatus. Gordon et al. (2012) attributed prolonged negative transport anomalies to diminished

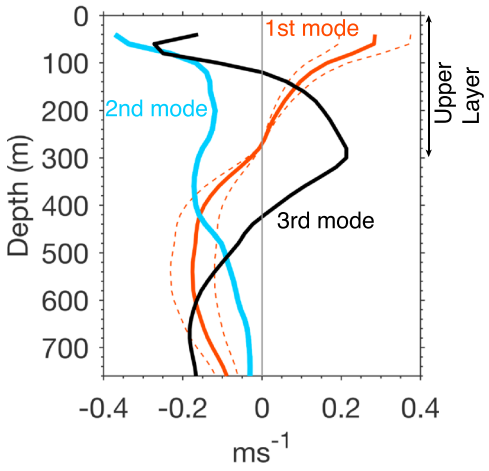

Figure 5. The vertical mode structures for the first three dominant modes of anomalies of the average v of the two moorings, inferred from an empirical orthogonal function analysis of the anomalies. The first (red), second (blue), and third (black) mode, respectively, accounts for 72%, 20%, and 5% of the anomalies. Dashed lines indicate 95% confidence limits attributed to the first mode.

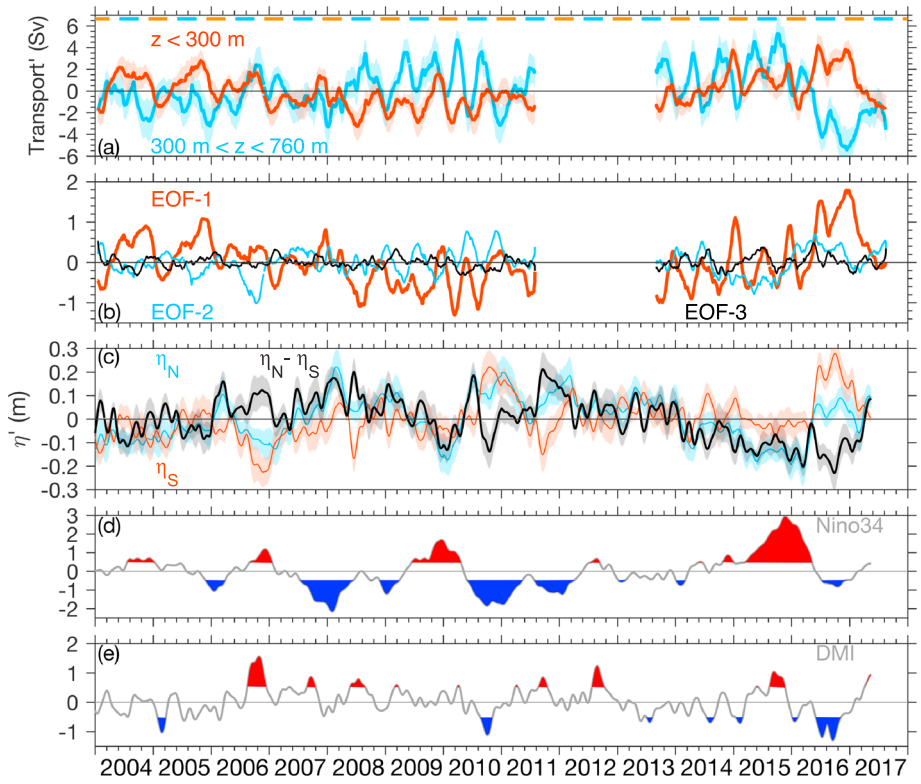

Figure 6. Daily time series of (a) total Indonesian Throughflow transport anomalies in the upper layer (red) and lower layer (blue), (b) amplitudes of the first three EOF modes of anomalies of the average v of the two moorings, (c) anomalies of $\delta\eta$, η_N, and η_S, (d) the NINO 3.4 index, and (e) the DMI observed between 2004 and 2017. Orange and blue horizontal bars in (a), respectively, indicate northwest monsoon months (December–March) and southeast monsoon months (June–September). Shaded red and blue areas in (d), respectively, indicate El Niño and La Niña events. Shaded red and blue areas in (e), respectively, mark positive and negative Indian Ocean dipole events. Daily DMI and NINO 3.4 index were smoothed with a 61-day triangle filter. EOF = empirical orthogonal function; DMI = Dipole Mode Index.

buoyant South China Sea's surface water entering the western Sulawesi Sea that resulted in suppressed eastward surface pressure head in Sulawesi Sea and hence intensified ITF transport into Makassar Strait. They argued that a series of La Niña events during 2007–2011 forced the reduced freshwater flux into Sulawesi Sea and subsequently the increased ITF transport that led an increase in heat flux into the Indian Ocean (Lee et al., 2015; Nieves et al., 2015). Positive IOD events also occurred during the extended period of negative ITF transport anomalies, which together with the series of La Niña events may set up a favorable condition for the observed intensification of mass transport of heat flux into the Indian Ocean.

Largest positive transport anomalies, indicating suppressed ITF transport, occurred over the course of boreal summer 2016, through which the upper layer transport showing a decrease by 2.5 ± 0.5 Sv, on average (Figures 6a and 7a). The positive ITF anomalies, particularly those peaked in July 2016, were unprecedented and yielded the weakest boreal summer ITF transport observed in the upper layer of Makassar Strait over the course of the observational period. The average magnitude of ITF seasonal transport in boreal summer for the upper layer was −8 ± 0.7 Sv (Figure 4a). A mean of +2.5 ± 0.5 Sv transport anomaly observed through summer 2016 thus reflected a 25–40% reduction of the upper layer ITF transport. The upper layer transport anomalies and the temporal modulation of the first EOF mode of the v anomalies across the upper 760 m (red curves in Figures 6a and 6b) appeared to be in phase and were significantly correlated ($r = 0.77 \pm 0.01, p < 0.001$). As expected, the transport anomalies in the lower layer generally were at out of phase with the upper layer, and they, like in the upper layer, were most notable in boreal summer and fall 2016 (blue curve in Figure 6a). Peaks of positive transport anomalies in the monsoon transition months, representing intrusions of Indian Ocean Kelvin waves into the Makassar Strait (Pujiana et al., 2013), typically characterized the ITF variation in the lower layer (Figure 6a). In 2016–2017, although the lower layer registered a mean of negative

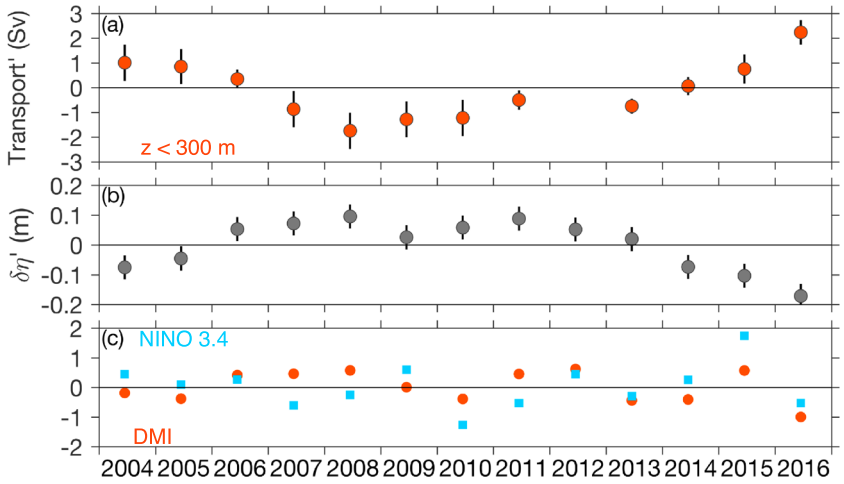

Figure 7. Averages of (a) total Indonesian Throughflow transport anomalies in the upper layer, (b) $\delta\eta$ anomalies, and (c) the DMI (red) and the NINO 3.4 index (blue) for the months of June–September over the course of 2004–2016. The averages were computed from the anomalies shown in Figure 6. Color coded vertical lines indicate 95% bootstrap confidence limits. DMI = Dipole Mode Index.

anomalies or an overall increase in ITF transport, the Kelvin waves markedly reduced the ITF transport by about 2–4 Sv.

Over the course of boreal summer to fall 2016, $\delta\eta$ attained its greatest negative anomalies, suggesting a substantial reduction of the interbasin pressure gradient (Figures 6c and 7b). Elevated η_S reversed the large-scale pressure gradient and thereby accounted for the negative anomalies of $\delta\eta$ over the anomalous period (Figure 6c). Interestingly, the anomalous ITF transport and $\delta\eta$ coincided with an extreme negative IOD event (Figures 6e and 7c), the strongest negative IOD event in the past decades (Lim & Hendon, 2017; Lu et al., 2017). A weak La Niña ($-1 < \text{NINO3.4} < -0.5$; Figure 6d) simultaneously occurred with the negative IOD, marked by positive anomalies of η_N (Figures 6c, 6d, and 2d). An increase of η over the western Pacific attributed to the weak La Niña event, however, was smaller compared to that off the southern coast of Java during the negative IOD event. Therefore, the La Niña 2016 did not dominate the suppressed $\delta\eta$ and by extension the reduced upper layer ITF transport. In principle, anomalies of ITF transport in the upper layer and $\delta\eta$ are significantly correlated (Figure 8), with $r = -0.8$ and $p < 0.001$, and the significant

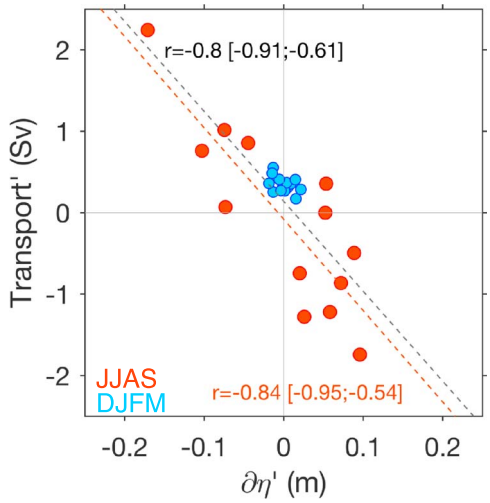

Figure 8. A scatter plot of anomalies of Indonesian Throughflow transport in the upper layer and $\delta\eta$ averaged over the months of June–September (JJAS, orange) and December–March (DJFM, blue) during 2004–2016. Dashed red and black lines, respectively, denote the least square line for the JJAS anomalies and the JJAS and DJFM anomalies combined. Values within the brackets indicate 95% confidence limits.

correlation is particularly governed by the anomalies during boreal summer (Figures 8, 7a, and 7b), demonstrating $r = -0.84$ and $p < 0.001$. A lower degree of correlation observed during boreal winter, $r = -0.5$ and $p < 0.01$, likely reflects impacts of interannual variation of South-China and Java Seas freshwater flux on the interbasin pressure gradient.

3.3. Relationships Between the Anomalies and ENSO/IOD

Figures 6 and 7 illustrate plausible links between ENSO, IOD, ITF transport, and pressure gradient anomalies, which explain the unprecedented reduction of the upper layer ITF transport observed during boreal summer 2016. Assessing impacts of large-scale interannual variations over the Indo-Pacific warm pools on the ITF has been mostly based on numerical experiments and ITF proxies (Masumoto, 2002; Meyers, 1996; Potemra & Schneider, 2007; Sprintall & Revelard, 2014). Studies that employ direct ITF measurements to evaluate the impacts are limited. Analyzing a subset of the Makassar Strait moored data that span from 2004 to mid-2011, Gordon et al. (2012) hypothesized that increased ITF transport during 2007–2009 was a response to prolonged La Niña periods. They also suggested that an El Niño event should typically suppress the ITF in Makassar Strait.

As a continuation of the study of Gordon et al. (2012), we here analyze the relationships between each ENSO and IOD and anomalies of ITF transport in the upper layer of Makassar Strait as well as the interbasin pressure gradient observed between January 2004 and July 2017. Through the observational period, El Niño and La Niña events each occurred four to six times with a similar recurrence rate for positive and negative IOD events (shaded area in Figures 6d and 6e). ENSO and IOD exhibited a significant correlation ($r = 0.3, p < 0.001$) over the course of 2004–2017, so a partial cross-correlation method (Saji & Yamagata, 2003) was employed to separate out ENSO impacts on IOD and vice versa when performing the linear regression of ITF transport and $\delta\eta$ anomalies on the DMI and NINO 3.4 index.

3.3.1. Pressure Gradient Anomalies Versus NINO 3.4 and DMI

The interocean pressure gradient responds distinctively to variations of each ENSO and IOD. A partial lagged cross correlation between the NINO 3.4 index and $\delta\eta$ anomalies indicates significant negative correlation coefficients at lags shorter than −360 days (~12 months), with the strongest correlation observed at around zero lag (blue curve in Figure 9a). The negative correlation with negative lags implies that an El Niño (La Niña) event may subsequently be followed by a reduced (increased) pressure gradient between the Pacific and Indian Oceans. It appears that the very strong fall 2015 to early 2016 El Niño (NINO3.4 > 2; Figure 6d) event weighs on the overall ENSO and $\delta\eta$ correlation for lags longer than −5 months (dashed curve in Figure 9a). This suggests that suppressed η_N during the very strong El Niño event that peaked in late 2015 unlikely led to the reduced $\delta\eta$ through summer to fall 2016 (Figures 6c and 6d).

The correlations between the NINO 3.4 index and each component constituting $\delta\eta$, η_N, and η_S provide insights into physical processes by which ENSO affects $\delta\eta$. η_N, respectively, drops and rises following an El Niño event and a La Niña event, and it lags an ENSO event by 1–5 months (blue curve of Figure 9b). The time lags may represent the period for an ENSO-forced Rossby wave typically needs to propagate along the equator from the central and eastern Pacific to the western boundary of the basin (Potemra & Lukas, 1999).

Similar to η_N, η_S anomalies are inversely correlated with the NINO 3.4 index variations, despite showing smaller correlation coefficients peaked at a lag time of −3 months (Figure 9c). Unlike η_N, the time lag shown by η_S does not likely indicate transmissions of Rossby waves of the Pacific origin, but it is rather indicative of Kelvin waves forced in the equatorial Indian Ocean in response to anomalous winds over the basin during ENSO. Surface wind divergent over the Indonesian maritime continent and easterly wind stress over the equatorial Indian Ocean that typically mark an El Niño period may enhance upwelling along the southern coasts of the Indonesian islands chain and force upwelling equatorial Kelvin waves that together suppress η_S. The opposite holds for a La Niña period.

A significant positive correlation between ENSO and η_S occurs at a lag time of about −10 months, likely related to the El Niño events in 2009 and 2015 and suppressed η_S during the 2010 La Niña event (Figures 9c, 6c, and 6d). The very strong 2015 El Niño event predominantly accounts for the correlation as excluding the event from the analysis lowers the degree of the correlation slightly below the significance level (dashed blue line in Figure 9c). Dynamically, the lag may be indicative of the time interval between the onset of ENSO-forced large-scale waves in the Indian Ocean and the arrival time of the waves off Sumatra and Java. Reflected off-equatorial downwelling Rossby waves, forced in response to El Niño-driven anticy-

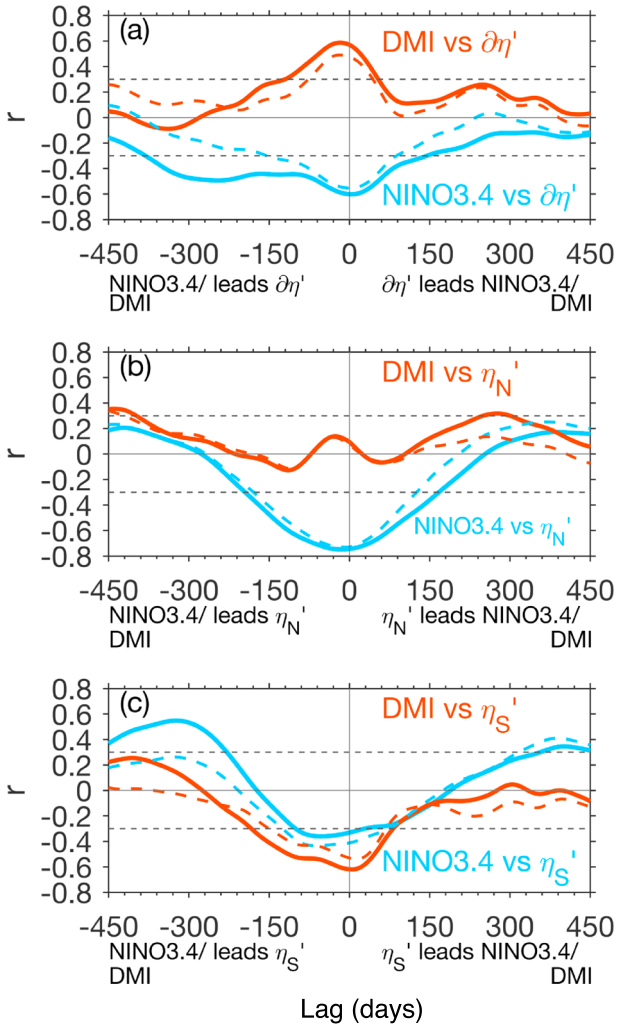

Figure 9. Lead-lag partial correlation of the DMI and NINO 3.4 index with $\delta\eta$ anomalies (a), η_N anomalies (b), and η_S anomalies (c). Solid curves indicate partial correlations that account for El Niño-Southern Oscillation and Indian Ocean dipole events occurring between January 2004 and July 2017; dashed curves exclude boreal fall 2015 to early 2016 El Niño for El Niño-Southern Oscillation and the boreal summer to fall 2016 during the negative Indian Ocean dipole event for the DMI. Horizontal dashed lines indicate 95% significance levels based on the method of Ebisuzaki (1997). DMI = Dipole Mode Index.

clonic winds centered at about 10° S in the Indian Ocean, may increase η off Sumatra and Java within a year following the onset of the El Niño (Jury & Huang, 2004; Murtugudde et al., 2000).

As for IOD, the DMI time series and $\delta\eta$ anomalies reveal a positive correlation skewed to negative lags between −4 months and zero lag, with a maximum correlation occurring at −1 month (red curve of Figure 9a). The correlation signifies increased pressure gradient that corresponds to a positive IOD, where SST off Java and Sumatra is colder than normal. Despite excluding the summer–fall 2016 negative IOD event from the cross-correlation computation, the significant correlation between the DMI variations and $\delta\eta$ anomalies still holds (dashed red curve of Figure 9a).

The dipole mode, as expected, exerts a strong influence on η_S anomalies (Figure 9c) but not so on η_N anomalies (Figure 9b). The DMI time series tends to lead η_S anomalies by up to 4 months (Figure 9c), with the largest correlations roughly centered at zero lag. The lags between η_S and DMI may suggest pulses of Kelvin waves originating in the western-central equatorial Indian, responding to anomalous equatorial winds attributed to IOD events. Anomalous easterlies typically prevail over the equatorial Indian Ocean through the development of positive IOD events, forcing trains of upwelling Kelvin waves that suppress η_S, whereas the opposite applies for negative IOD events (Delman et al., 2016; Yan et al., 2012). It would take

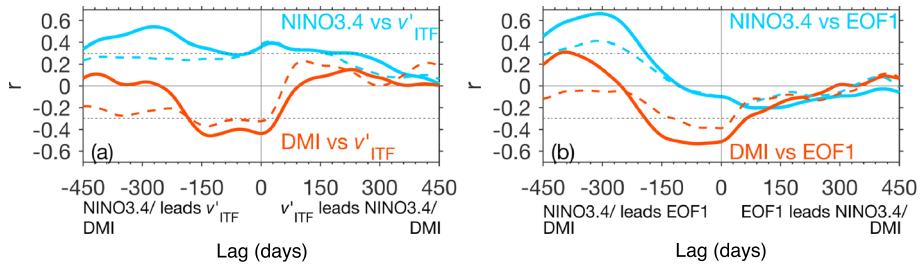

Figure 10. Lead-lag partial correlation of NINO 3.4 and DMI with ITF transport anomalies (v'_{ITF}) in the upper layer (a) and principal component time series of the leading empirical orthogonal function mode of anomalies of the average v of the two moorings in the upper 760 m (b). Solid curves indicate partial correlations that account for El Niño-Southern Oscillation and Indian Ocean dipole events occurring between January 2004 and July 2017; dashed curves exclude boreal fall 2015 to early 2016 El Niño for El Niño-Southern Oscillation and the boreal summer to fall 2016 during the negative Indian Ocean dipole event for the DMI. Horizontal dashed lines indicate 95% significance levels based on the method of Ebisuzaki (1997). DMI = Dipole Mode Index; ITF = Indonesian Throughflow.

about 11 days to 4 months for a Kelvin wave with phase speeds varying between 0.5 and 3 ms^{-1}, the typical speeds for equatorial Kelvin wave with the gravest baroclinic modes (Iskandar et al., 2005), to traverse along the equatorial waveguide from the eastern coast of Africa to the western coast of Sumatra.

3.3.2. ITF Anomalies Versus NINO 3.4 and DMI

In the upper layer, ENSO and IOD are significantly correlated with ITF transport anomalies. The NINO 3.4 index and the transport anomalies exhibit a maximum positive correlation, with ENSO leading the ITF by about 270 days (~9 months), implying the upper layer of Makassar Strait should experience a decrease (increase) of ITF transport about 9 months after an El Niño (La Niña) event associated with colder (warmer) than normal SST over the western Pacific (solid blue curve in Figure 10a). However, the maximum correlation at about −9 months does not statistically hold when the ITF transport anomalies and the NINO 3.4 index over the course of the strong fall 2015 to early 2016 are excluded from the partial cross-correlation analysis (dashed blue curve in Figure 10a). At shorter time lags, the ITF transport anomalies are also statistically correlated with the NINO 3.4 index, roughly between −1 month and zero lag, albeit with a smaller correlation coefficient (Figure 10a).

As for the IOD, the DMI and ITF transport anomalies in the upper layer were negatively correlated (solid red curve in Figure 10a). Although the negative IOD 2016 event is subtracted from the partial correlation computation, the degree of correlation between DMI and ITF transport anomalies in the upper layer is still above the 95% significance level (dashed red curve in Figure 10a). The significant negative correlation implies that a negative IOD event, when the southeastern Indian Ocean is warmer than normal, leads to weakened ITF transport and vice versa for a positive IOD. Similar to $\delta\eta$, the ITF transport anomalies respond to the DMI immediately or with lags varying up to 5 months. While the immediate response of the transport anomalies to IOD is expected, the lagged response may reflect impacts of equatorially and off Sumatra sourced Kelvin waves on $\delta\eta$ and hence the ITF.

Important contributions of IOD and ENSO to ITF in the upper layer in Makassar Strait are further confirmed by the partial cross correlations between the principal component time series of the leading EOF mode of anomalies of the average v profile of the two moorings and the NINO 3.4 and DMI. The leading EOF mode, accounting for 72% of the average v anomalies in the upper 760 m of Makassar Strait, is more significantly correlated with IOD than ENSO, with the DMI leading the average v anomalies by 0–5 months (red curves of Figure 10b). The imprint of ENSO on the bulk of the average v anomalies is more pronounced at longer lags centered at about −10 months, and it is significant even for the scenario excluding the data attributed to the big 2015 El Niño from the cross-correlation computation (Figure 10b). As discussed, the lags could represent influential contribution of ENSO-forced large-scale waves in the Indian Ocean to the ITF, predominantly observed in the lower layer of Makassar Strait (Pujiana et al., 2013).

4. Relation of Upper Layer ITF Variations to Basin-Scale Indian Ocean Anomalies

Results from the partial correlations between ITF transport anomalies in Makassar Strait, the interocean pressure gradient, the NINO 3.4 index, and DMI, discussed above, provide preliminary insights into the

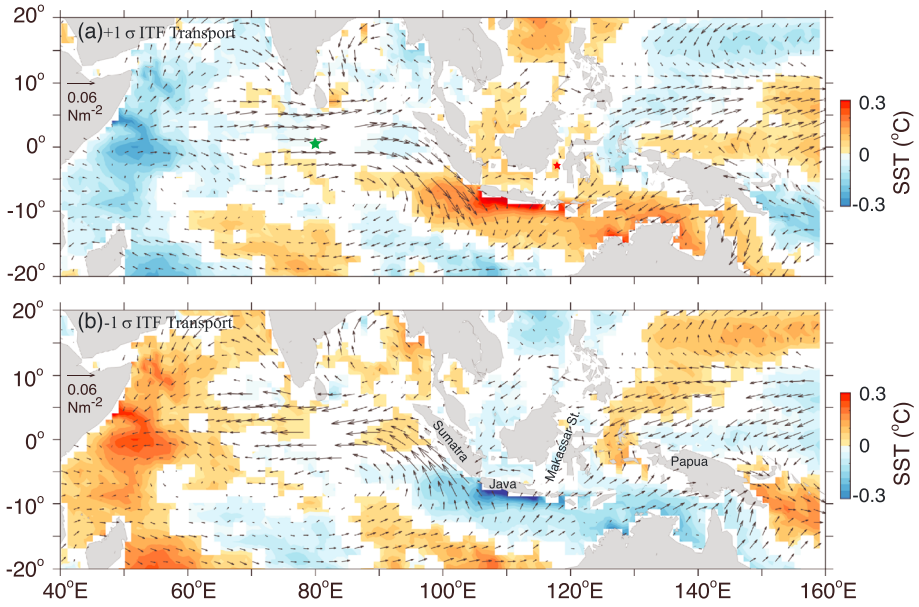

Figure 11. SST and τ anomalies regressed against ITF transport anomalies in the upper layer (above 300 m) of the Makassar Strait observed at zero-lag during months of June–November over the years of 2004–2017 for (a) transport equal to +1 standard deviation or 1.6 Sv and (b) transport equal to −1 standard deviation or −1.6 Sv. Green star in (a) denotes a Research Moored Array for African-Asian-Australian Monsoon Analysis and Prediction mooring at 0°, 80° E in the central equatorial Indian Ocean, and red star denotes a Makassar Strait mooring. Only regressions significant at 80% level are shown. ITF = Indonesian Throughflow; SST = sea surface temperature.

relationship between ITF and both ENSO and IOD. The correlations point to the role of ENSO and IOD in modulating the pressure gradient and ITF transport anomalies. To further explore the relationships, the correlations between the transport anomalies and satellite-derived SST, η, surface winds, and currents anomalies over a broader Indo-Pacific region are analyzed. Capturing the relationships between the transport anomalies in the upper layer and the satellite-retrieved data, which illustrate basin-scale spatial structure of either IOD or ENSO, is the focus.

A regression analysis between ITF transport anomalies in the upper layer and SST as well as wind stress anomalies for the months of June through November reveals the imprint of IOD on the ITF (Figure 11). Figure 11a illustrates that a positive ITF transport anomaly, that is, a reduced ITF transport, in the upper layer of Makassar Strait corresponds with a basin-scale pattern of SST associated with a negative IOD event, in which SST is warmer by up to 0.3 °C over the southeastern Indian Ocean and colder by a similar amount over western tropical Indian Ocean and off the eastern coast of Africa. The typical SST dipole mode is corroborated by prevailing westerlies across the tropical Indian Ocean and anticyclonic winds over the Bay of Bengal, inherent characteristics of a negative IOD event (Schott et al., 2009; Thompson et al., 2006). Conversely, intensified upper layer ITF transport into the Indian Ocean occurs in association with a positive IOD, where SST over the southeastern Indian Ocean is colder and τ along the equatorial Indian Ocean and over the Bay of Bengal turns easterlies and anticyclonic (Figure 11b). Note that the regression analysis was done for the months of June to November, instead of September to November through which the largest amplitudes of the IOD are typically observed (McPhaden et al., 2015), to take into account IOD events occurring through boreal summer. However, a regression analysis using September to November ITF data reveals similar spatial structures of SST and τ attributed to the IOD.

Regressed η and surface currents onto the ITF transport anomalies also demonstrate broad-scale signatures reminiscent of IOD patterns. For a negative IOD event in association with anomalously negative ITF transport, high η prevails in the eastern and southeastern Indian Ocean, and surface currents near the equator are generally eastward and bifurcate poleward off Sumatra (Figure 12a). Eastward surface currents near the equator, related to the Wyrtki jets, transport water eastward where it converges against the coast of Sumatra, hence elevating η there. Depressed η and its respective anticyclonic flow also mark the broad-scale signatures. Opposite conditions apply for a positive IOD event (Figure 12b). These signatures are consistent

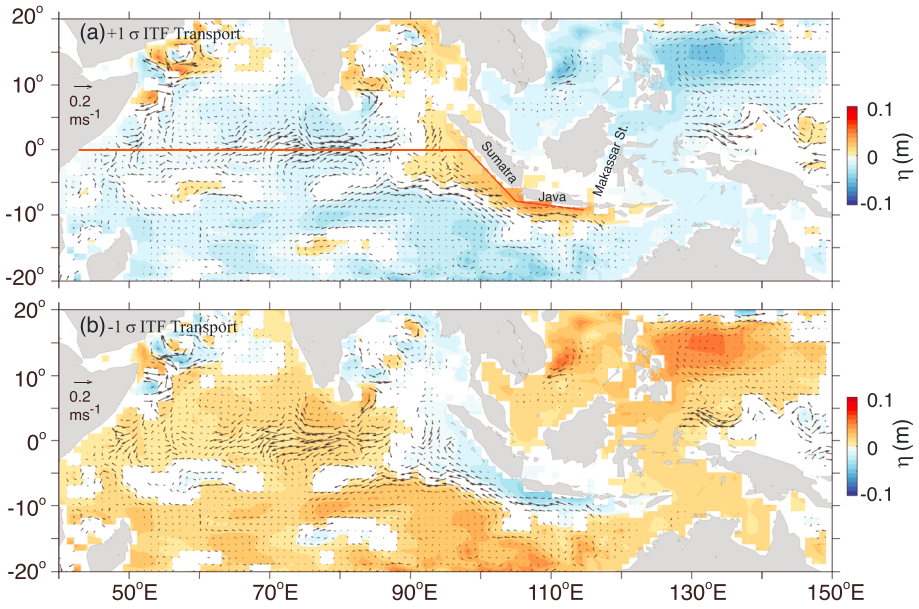

Figure 12. Ocean Surface Current Analysis Real Time surface current and η anomalies regressed against total ITF transport anomalies in the upper layer of Makassar Strait observed during months of June–November over the years of 2004–2017. (a) demonstrates the zero-lag regression for transport equal to +1 standard deviation or 1.6 Sv and (b) as in (a) but for transport equal to −1 standard deviation or −1.6 Sv. Only regressions significant at 80% level are shown. Red line illustrates a Kelvin wave pathway extending from the eastern coast of Africa to the southern coast of Java, at which η anomalies shown in Figure 15 are analyzed. ITF = Indonesian Throughflow.

with the typical IOD patterns inferred from the equatorial RAMA moorings (McPhaden et al., 2015). Strong Wyrtki jets, in response to westerly winds associated with negative IOD events, are observed in the equatorial RAMA mooring at 80° E (Figure 13). The boreal spring 2016 Wyrtki jet, occurring through the initiation of the 2016 negative IOD event, was the strongest in the record (Figure 13b).

ITF transport anomalies are linked to broad-scale signatures attributed to IOD (Figures 12 and 13). Equatorial winds and their respective surface currents are among the distinct signatures closely associated with the transport anomalies. To further explore the links between equatorial dynamics in the Indian Ocean and

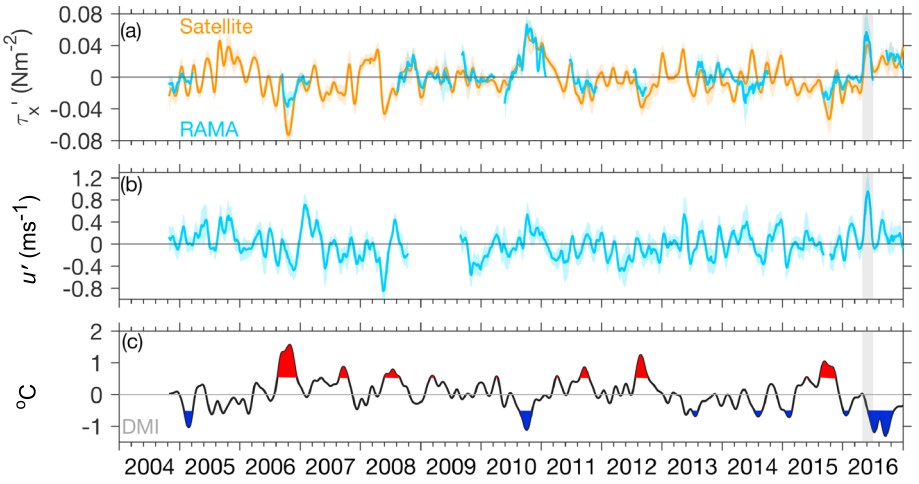

Figure 13. Time series of daily anomalies of (a) satellite-derived (orange) and moored (blue) zonal wind stress, τ_x (blue), (b) u averaged in the upper 80 m at 0°, 80° E, and (c) the DMI observed between 2004 and 2017. The satellite-derived, moored, and DMI time series was smoothed with a 61-day triangle filter. Shaded gray areas mark April–May 2016. Shaded red areas in (c) indicate positive Indian Ocean dipole events, while shaded blue areas mark negative Indian Ocean dipole events. RAMA = Research Moored Array for African-Asian-Australian Monsoon Analysis and Prediction; DMI = Dipole Mode Index.

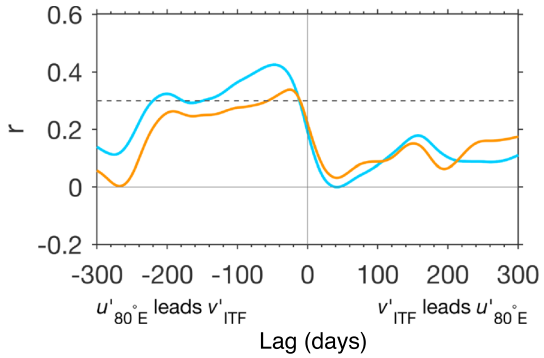

Figure 14. Lead-lag partial correlation of anomalies of u averaged in the upper 80 m at the Research Moored Array for African-Asian-Australian Monsoon Analysis and Prediction 0°, 80° E ($u'_{80°E}$) mooring and those of ITF transport (v'_{ITF}) in the upper layer observed through January 2004 to July 2017. Blue and orange curves, respectively, illustrate the correlation for v'_{ITF} anomalies averaged in the upper 80 and 300 m. ITF = Indonesian Throughflow.

ITF anomalies, we sought the relationships between anomalies of zonal velocity averaged in the upper 80 m observed at the RAMA 0°, 80° E mooring (henceforth referred to as surface layer $u'_{80°E}$) and that of ITF transport in Makassar Strait. Analyzing data extending from 2004 to 2013 from an array of RAMA moorings at 80° E, McPhaden et al. (2015) reported a relationship between IOD and surface layer zonal transport at the equatorial Indian Ocean, highlighting pronounced impacts of anomalous zonal winds associated with IOD on the strength of the Wyrtki jets, particularly the northern fall jet.

In 2016, the influential impact of IOD on the Wyrtki jets was more pronounced through the IOD's initiation phase. Surface layer $u'_{80°E}$ was most energetic at the equatorial mooring in May to early June 2016, in response to anomalously strong easterly winds (Figures 13a and 13b). The spring 2016 Wyrtki jet marked the most energetic surface layer $u'_{80°E}$ ever recorded at the mooring site through the observational period, and it occurred about a few weeks prior to the peak of the negative IOD event (Figure 13c). It was succeeded by events of eastward surface layer $u'_{80°E}$ through the IOD event (Figure 13b). The surface layer $u'_{80°E}$ and ITF transport anomalies in the upper layer are statistically correlated with the $u'_{80°E}$ leading the transport anomalies by a time lag varying between 1 and 4 months (Figure 14). Assuming a path with a distance of about 5,000 km connects the RAMA and Makassar moorings, the time lag implies a propagation from the central equatorial Indian Ocean to Makassar Strait with a phase speed of around 0.5–2 ms^{-1}.

Dynamically, the eastward phase speeds of 0.5–2 ms^{-1} inferred from the lagged correlation between surface layer $u'_{80°E}$ and ITF transport anomalies in the upper layer indicate the importance of large-scale equatorial Kelvin waves in affecting surface layer zonal currents in the equatorial Indian Ocean, including the Wyrtki jets (Nagura & McPhaden, 2010a, 2010b). In order to explore equatorial wave influences on the ITF transports in more detail, we analyzed η anomalies along a transect extending from the east coast of equatorial Africa to off Java (red line in Figure 12a). The leading mode of the complex EOF of the η anomalies, accounting for 80% of the anomalies, shows that the anomalies increase to the east (Figure 15a). The first complex EOF mode phase also increases to the east (Figure 15b), implying an eastward propagation, consistent with

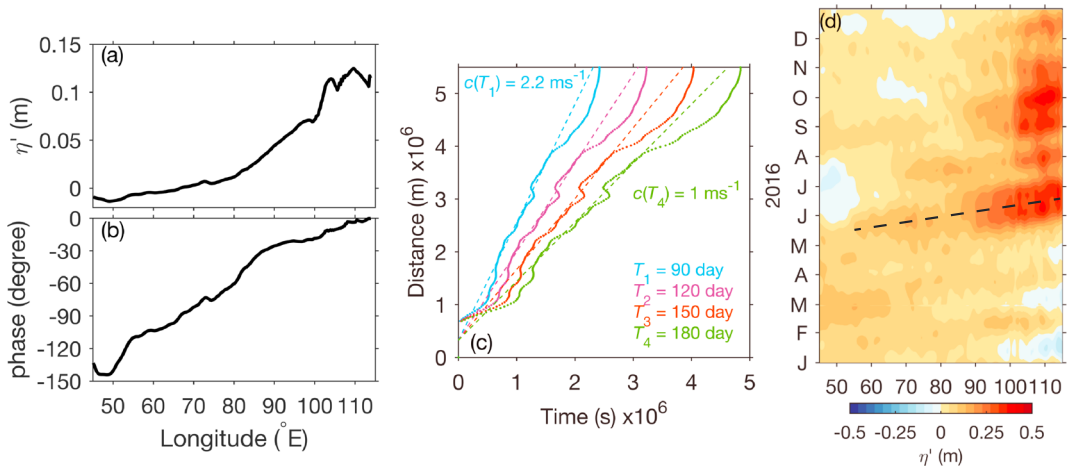

Figure 15. Amplitude (a) and phase (b) of the leading complex empirical orthogonal function mode of η anomalies during 2004–2017 along the equatorial/coastal waveguide shown as the red line in Figure 12a. The amplitude and phase were, respectively, determined from the eigenvector (v) of the mode, obtained from the complex empirical orthogonal function analysis, at each longitude along the waveguide as $\sqrt{v(v-iv)}$ and $\tan^{-1}(iv/v)180/\pi$. The mode accounts for 80% of the η anomalies. (c) Time-distance plots inferred from (a) for periods of 90 (blue), 120 (magenta), 150 (red), and 180 days (green). Color coded c indicates phase speed. (d) Longitude-time plot of η anomalies in 2016. Slanted dashed line marks a downwelling Kelvin wave propagating eastward along the waveguide in May 2016.

that inferred from the correlation between surface layer $u'_{80°E}$ and ITF transport anomalies. This eastward phase speed is consistent with the idea that along the equator on subseasonal to seasonal and longer time scales, sea level variations are more strongly influenced by Kelvin waves than Rossby (Nagura & McPhaden, 2010a).

Using the mode's phase, we determined that the phase speeds of eastward propagation at semiannual time scales vary between 1 and 1.3 ms^{-1} (Figure 15c), which commensurate with the phase speeds of equatorial Kelvin waves of the second or higher baroclinic modes (Jensen, 1993; Nagura & McPhaden, 2010b). Analyses of monthly η from tide gauge stations along the coast of Sumatra and Java suggested that the second vertical mode predominantly accounted for η variations on semiannual time scales there (Clarke & Liu, 1993). Pulses of downwelling Kelvin waves propagating along the waveguide extending from the equator to off Java and Sumatra were evident in η anomalies during the development of the IOD event in 2016 (Figure 15d). Furthermore, the bulk of ITF transport anomalies demonstrate a vertical structure of the second baroclinic mode. Thus, it appears that equatorial Kelvin waves, transformed into coastal Kelvin waves off Sumatra and Java, modulate the Pacific to Indian Ocean pressure gradient and hence the ITF transport.

5. Summary and Discussion

Long-term observations in Makassar Strait during 2004 to mid-2011 and August 2013 to July 2017 revealed a notable change in ITF transport across the upper layer (surface to 300 m) in June–September 2016, during which the transport on average was reduced by an unprecedented 25–40%. This anomalously attenuated ITF transport, resulting in the weakest boreal summer transport over the course of the observations, has provided a new insight into the complexity of ITF variability.

Through analyses of the ITF measurements in Makassar Strait, data from a RAMA mooring in the central equatorial Indian Ocean, and a suite of satellite-derived data over the Indo-Pacific region observed between 2004 and mid-2017, we attempt to assess whether the anomalous ITF is linked to variations of large-scale climatic forcing in the Indo-Pacific region such as ENSO and IOD. Our results can be summarized as follows.

1. Seasonal cycles and their anomalies of $\delta\eta$ between the western Pacific and off Sumatra and Java predominantly dictate anomalies of upper layer ITF transport in Makassar Strait, whereby $\delta\eta$ accounts for about 64% of the ITF transport variance, a percentage inferred from their cross correlation given in Figures 4c and 8. Largest anomalies of $\delta\eta$ and the ITF transport over the past decade occurred in June–September 2016, during which the transport was reduced by 25–40%. The anomalous $\delta\eta$ and ITF co-occurred with a negative IOD and a weak La Niña.
2. Anomalies of the upper layer ITF transport and $\delta\eta$ demonstrate a significant correlation with the DMI, with time lags of 0–5 months suggesting a negative IOD event leads to a decrease in ITF transport and interocean pressure gradient, while a positive IOD event leads to an increase in ITF transport and interocean pressure gradient. The leading vertical EOF mode of anomalies of the average v of the two moorings in the upper 760 m, accounting for 72% of the variance attributed to the anomalies, exhibits a similar correlation with the DMI.
3. Anomalies of the upper layer ITF transport are significantly correlated with those of $u'_{80°E}$ averaged in the upper 80 m in the central equatorial Indian Ocean at a lag of 1–4 months, implying anomaly propagation toward Makassar Strait with a phase speed of 0.5–2 ms^{-1}. Sea level anomalies on a Kelvin wave pathway extending along the Indian Ocean equator and the southern coast Sumatra and Java also reveal eastward propagation with similar phase speeds. The lag hence indicates an influential role of the Indian Ocean, via predominantly second baroclinic Kelvin waves, in modulating $\delta\eta$ and consequently the ITF transport in Makassar Strait. Surface layer $u'_{80°E}$ and η anomalies revealed an unprecedentedly strong spring Wyrtki jet and downwelling Kelvin wave preceding the negative IOD in summer 2016.
4. Regressed anomalies of satellite-derived SST, η, and surface τ against those of the upper layer ITF transport at zero lag for the months of June through November exhibit a spatial scale reminiscent to IOD. Reduced ITF transports commensurate with basin-scale patterns of SST and τ attributed to a negative IOD event, marked by warmer SST and higher η than normal over the southeastern Indian Ocean and prevailing westerlies and eastward surface currents across the equatorial Indian Ocean. Opposite conditions associated with a positive IOD event would lead to increased ITF transports.
5. Influenced by the strong 2015–16 El Niño, anomalies in the upper layer ITF transport and $\delta\eta$ are positively correlated the NINO 3.4 index, with NINO 3.4 leading by about 9–10 months. This relationship

implies that an El Niño (La Niña) event leads to a decreased (increased) ITF transport via the formation of ENSO wind-forced long Rossby waves radiation affecting the western Pacific. The $\delta\eta$ and ITF transport anomalies are also weakly and positively correlated with the NINO 3.4 index, with the index leading by 0–4 months. Our interpretation of this relationship is that the anomalously reduced ITF transport in the upper layer during boreal summer 2016 is a response to the negative IOD, not to the concurrently weak La Niña.

Our observations indicate that about 72% of the variance of ITF transport anomalies exhibit a two-layer vertical structure, the upper and lower layers, with a 10°C isotherm demarcating the upper from the lower (Gordon et al., 2019). The transport anomalies in both layers generally demonstrate an opposite sign, implying a decrease in ITF transport in the upper layer coincides with an increase in the lower layer and vice versa. The upper layer transport anomalies were clearly out of phase with the lower layer transport anomalies through June–November 2016, coinciding with the anomalously strong negative IOD event, during which the ITF transports were simultaneously reduced in the upper layer and increased in the lower.

The two-layer system shown by the bulk of ITF transport anomalies, in which the sign of the ITF transport in the upper layer differs from that in the lower layer, might be reflective of the influence of oceanic processes in the equatorial Indian Ocean on the transport anomalies. Nagura and McPhaden (2010a) posited that interannual variations of zonal velocity in the equatorial Indian Ocean were dominated by the second baroclinic mode, with the upper most zero-crossing depth at about 200 m. Furthermore, Clarke & Liu (1993, 1994) suggested that the second baroclinic mode predominantly accounted for anomalies on semiannual to annual time scales on the eastern boundaries of the Indian Ocean. Their results, coupled with our finding demonstrating significant correlations between surface layer zonal current anomalies at the central equatorial Indian Ocean and ITF transport anomalies, are indicative of the role of the second baroclinic Kelvin waves in dictating the large-scale pressure head and hence two-layer system of the ITF transport anomalies.

The remaining 20% of the variance of ITF transport anomalies exhibit a vertical structure with a uniform sign across the upper 760 m. Gordon et al. (2019) reported a historical high of total ITF transport in Makassar Strait, amounting of 20 Sv, in the first half 2017, coinciding with increased negative transport anomalies across depth, particularly in the lower layer. Underlying physical processes explaining the high total transport in 2017 remains to be investigated (Gordon et al., 2019).

Using ITF geostrophic transport estimated from repeated expendable bathythermograph data along the IX1 section between Fremantle-Australia and Sunda Strait-Indonesia during 1980–2013, Liu et al. (2015) showed a delayed ITF response to ENSO varying between 4- and 11-month lag, peaking at 7 months, with the ITF geostrophic transport decreasing in response to El Niño and increasing response to La Niña. Applying the delayed ITF response to the boreal fall 2015 to early 2016 strong El Niño case, the 7-month lag suggests the influence of upwelling equatorial upwelling Rossby waves forced by the wind anomalies associated with the El Niño in the Pacific Ocean, which would have lowered η_N, reduced the interbasin pressure force, and thus contributed to the reduction in ITF transport in the summer to fall 2016. Nevertheless, the weak La Niña was more influential than the El Niño-related upwelling Rossby waves on η_N that exhibited a net increase in the western Pacific during the summer to fall 2016. Yet, despite an increased η_N, the extreme negative IOD was the ultimate determinant of the interbasin pressure force anomaly toward the Pacific Ocean, accounting for the unprecedented reduction in ITF transport during summer 2016.

When a negative IOD and La Niña co-occur, the extent to which the negative IOD event affects the ITF transport in the upper layer depends on the relative strengths of the La Niña and IOD events. For example, a negative IOD developed in September–October 2010, while ITF transport in the upper layer on average was enhanced by -1.5 ± 0.9 Sv, in contrast to what happened during the negative IOD event in 2016. The overall increase in the ITF transport during the negative IOD event in 2010 was likely due to the intensity of the La Niña that developed from a moderate ($-1.5 <$ Nino 3.4 < -1) to a strong ($-2 <$ Nino 3.4 < -1.5) event from boreal summer to fall. Determining what factors contribute to the dominance of co-occurring negative IOD events over a La Niña events, or vice versa, requires analysis of more concurrent negative IOD-La Niña cases, which is beyond the scope of this study.

Mayer et al. (2018), using reanalysis products, posited that ITF transport was greatly reduced during 2015–2016 and that this reduction was due to a substantial warming of the eastern Indian Ocean on decadal variability time scales. Here we argue that the reduced ITF transport in the upper layer in 2016 is a response

to the extreme negative IOD event which may be sparked by the preceding boreal fall 2015 to early 2016 strong El Niño. Lim and Hendon (2017) hypothesized that El Niño-forced anticyclonic winds centered at around 10° S in the Indian Ocean caused the genesis of downwelling Rossby waves that propagated westward and turned into downwelling Kelvin waves once hitting the eastern coast of Africa. They further argued that the downwelling Kelvin waves facilitated a stronger Bjerknes feedback during the initiation of the negative IOD event by warming the eastern Indian Ocean that consequently increased the zonal gradient of SST and further intensified westerly winds.

Acknowledgments
We appreciate important contributions of Aryo Hanggono, Ngurah Wiadyana, Agus Setiawan, Nurman Mbay, and Anastasia Tisiana of Ministry of Marine Affairs and Fisheries of the Republic of Indonesia for making arrangements to service the Makassar Strait mooring. We also acknowledge NOAA and its partners for maintaining the RAMA moored buoy array and Bruce Huber of LDEO for initial processing the Makassar Strait mooring data. Constructive comments from two anonymous reviewers on an earlier version of the manuscript are appreciated. The Makassar Strait data can be accessed online (http://ocp.ldeo.columbia.edu/res/div/ocp/projects/MITF/cmdata/) and the RAMA data can be downloaded online (https://www.pmel.noaa.gov/tao/drupal/disdel/). This research was performed while the first author held a National Research Council Research Associateship Award at NOAA/PMEL. M. J. M. is supported by NOAA; A. L. G. and A. M. N. were supported by NOAA UCAR Z15-17551. This is PMEL contribution 4828. LDEO contribution 8286.

References

Bentamy, A., Katsaros, K., Drennan, W., & Forde, E. (2002). Daily surface wind fields produced by merged satellite data. *Gas Transfer at Water Surfaces*, *127*, 343–349.

Bonjean, F., & Lagerloef, G. S. (2002). Diagnostic model and analysis of the surface currents in the tropical Pacific Ocean. *Journal of Physical Oceanography*, *32*(10), 2938–2954.

Clarke, A. J., & Liu, X. (1993). Observations and dynamics of semiannual and annual sea levels near the eastern equatorial Indian Ocean boundary. *Journal of Physical Oceanography*, *23*(2), 386–399. https://doi.org/10.1175/1520-0485(1993)023<0386:Oadosa>2.0.Co;2

Clarke, A. J., & Liu, X. (1994). Interannual sea-level in the northern and eastern Indian Ocean. *Journal of Physical Oceanography*, *24*(6), 1224–1235.

Delman, A. S., Sprintall, J., McClean, J. L., & Talley, L. D. (2016). Anomalous Java cooling at the initiation of positive Indian Ocean Dipole events. *Journal of Geophysical Research: Oceans*, *121*, 5805–5824. https://doi.org/10.1002/2016JC011635

Dong, L., & McPhaden, M. J. (2016). Interhemispheric SST Gradient Trends in the Indian Ocean prior to and during the Recent Global Warming Hiatus. *Journal of Climate*, *29*(24), 9077–9095. https://doi.org/10.1175/jcli-d-16-0130.1

Ducet, N., Le Traon, P.-Y., & Reverdin, G. (2000). Global high-resolution mapping of ocean circulation from Topex/Poseidon and ERSA-1 and -2. *Journal of Geophysical Research*, *105*(C8), 19477–19498.

Ebisuzaki, W. (1997). A method to estimate the statistical significance of a correlation when the data are serially correlated. *Journal of Climate*, *10*(9), 2147–2153. https://doi.org/10.1175/1520-0442(1997)010<2147:Amtets>2.0.Co;2

England, M. H., McGregor, S., Spence, P., Meehl, G. A., Timmermann, A., Cai, W., et al. (2014). Recent intensification of wind-driven circulation in the Pacific and the ongoing warming hiatus. *Nature Climate Change*, *4*(3), 222.

Godfrey, J. S. (1996). The effect of the Indonesian Throughflow on ocean circulation and heat exchange with the atmosphere: A review. *Journal of Geophysical Research*, *101*(C5), 12217–12237.

Gordon, A. L. (1986). Inter-ocean exchange of thermocline water. *Journal of Geophysical Research*, *91*(C4), 5037–5046.

Gordon, A. L., & Fine, R. A. (1996). Pathways of water between the Pacific and Indian Oceans in the Indonesian seas. *Nature*, *379*(6561), 146–149.

Gordon, A. L., Huber, B. A., Metzger, E. J., Susanto, R. D., Hurlburt, H. E., & Adi, T. R. (2012). South China Sea Throughflow impact on the Indonesian Throughflow. *Geophysical Research Letters*, *39*, L11602. https://doi.org/10.1029/2012GL052021

Gordon, A. L., Sprintall, J., Van Aken, H. M., Susanto, D., Wijffels, S., Molcard, R., et al. (2010). The Indonesian Throughflow during 2004-2006 as observed by the INSTANT program. *Dynamics of Atmospheres and Oceans*, *50*(2), 115–128.

Gordon, A. L., Susanto, R. D., & Ffield, A. (1999). Throughflow within Makassar Strait. *Geophysical Research Letters*, *26*(21), 3325–3328.

Gordon, A. L., Susanto, R. D., Ffield, A., Huber, B. A., Pranowo, W., & Wirasantosa, S. (2008). Makassar Strait Throughflow, 2004 to 2006. *Geophysical Research Letters*, *35*, 24605. https://doi.org/10.1029/2008GL036372

Gordon, A. L., Napitu, A., Huber, B. A., Gruenburg, L. K., Pujiana, K., Agustiadi, T., et al. (2019). Makassar strait throughflow seasonal and interannual variability, an overview. *Journal of Geophysical Research: Oceans*, *124*. https://doi.org/10.1029/2018JC014502

Ilahude, A. G., & Gordon, A. L. (1996). Thermocline stratification within the Indonesian seas. *Journal of Geophysical Research*, *101*(C5), 12,401–12,409.

Iskandar, I., Mardiansyah, W., Masumoto, Y., & Yamagata, T. (2005). Intraseasonal Kelvin waves along the southern coast of Sumatra and Java. *Journal of Geophysical Research*, *110*, C04013. https://doi.org/10.1029/2004JC002508

Jensen, T. G. (1993). Equatorial variability and resonance in a wind-driven Indian Ocean model. *Journal of Geophysical Research*, *98*(C12), 22533–22552. https://doi.org/10.1029/93jc02565

Jury, M. R., & Huang, B. H. (2004). The Rossby wave as a key mechanism of Indian Ocean climate variability. *Deep-Sea Research Part I-Oceanographic Research Papers*, *51*(12), 2123–2136. https://doi.org/10.1016/j.dsr.2004.06.005

Kosaka, Y., & Xie, S.-P. (2013). Recent global-warming hiatus tied to equatorial Pacific surface cooling. *Nature*, *501*(7467), 403.

L'Heureux, M. L., Takahashi, K., Watkins, A. B., Barnston, A. G., Becker, E. J., Di Liberto, T. E., et al. (2017). Observing and predicting the 2015/16 El Niño. *Bulletin of the American Meteorological Society*, *98*(7), 1363–1382.

Lee, T., Fukumori, I., Menemenlis, D., Xing, Z. F., & Fu, L. L. (2002). Effects of the Indonesian Throughflow on the Pacific and Indian Oceans. *Journal of Physical Oceanography*, *32*(5), 1404–1429.

Lee, S., Park, W., Baringer, M. O., Gordon, A. L., Huber, B., & Liu, Y. (2015). Pacific origin of the abrupt increase in Indian Ocean heat content during the warming hiatus. *Nature Geoscience*, *8*(6), 445.

Lim, E.-P., & Hendon, H. H. (2017). Causes and predictability of the negative Indian Ocean Dipole and its impact on La Niña during 2016. *Scientific Reports*, *7*(1), 12619.

Liu, Q. Y., Feng, M., Wang, D. X., & Wijffels, S. (2015). Interannual variability of the Indonesian Throughflow transport: A revisit based on 30 year expendable bathythermograph data. *Journal of Geophysical Research: Oceans*, *120*, 8270–8282. https://doi.org/10.1002/2015JC011351

Lu, B., Ren, H.-L., Scaife, A. A., Wu, J., Dunstone, N., Smith, D., et al. (2017). An extreme negative Indian Ocean Dipole event in 2016: Dynamics and predictability. *Climate Dynamics*, *51*, 1–12.

Masumoto, Y. (2002). Effects of interannual variability in the eastern Indian ocean on the Indonesian Throughflow. *Journal of Oceanography*, *58*(1), 175–182.

Masumoto, Y., & Yamagata, T. (1996). Seasonal variations of the Indonesian throughflow in a general ocean circulation model. *Journal of Geophysical Research*, *101*(C5), 12287–12293.

Mayer, M., Alonso Balmaseda, M., & Haimberger, L. (2018). Unprecedented 2015/2016 Indo-Pacific heat transfer speeds up tropical Pacific heat recharge. *Geophysical Research Letters*, *45*, 3274–3284. https://doi.org/10.1002/2018GL077106

McPhaden, M. J., Meyers, G., Ando, K., Masumoto, Y., Murty, V. S. N., Ravichandran, M., et al. (2009). RAMA the research moored array for African-Asian-Australian monsoon analysis and prediction. *Bulletin of the American Meteorological Society*, *90*(4), 459–480.

McPhaden, M. J., Wang, Y., & Ravichandran, M. (2015). Volume transports of the Wyrtki jets and their relationship to the Indian Ocean Dipole. *Journal of Geophysical Research: Oceans*, *120*, 5302–5317. https://doi.org/10.1002/2015JC010901

Meyers, G. (1996). Variation of Indonesian Throughflow and the El Niño Southern Oscillation. *Journal of Geophysical Research*, *101*(C5), 12255–12263.

Murtugudde, R., Busalacchi, A. J., & Beauchamp, J. (1998). Seasonal-to-interannual effects of the Indonesian throughflow on the tropical Indo-Pacific basin. *Journal of Geophysical Research*, *103*(C10), 21425–21441.

Murtugudde, R., McCreary, J. P., & Busalacchi, A. J. (2000). Oceanic processes associated with anomalous events in the Indian Ocean with relevance to 1997–1998. *Journal of Geophysical Research*, *105*(C2), 3295–3306.

Nagura, M., & McPhaden, M. J. (2010a). Dynamics of zonal current variations associated with the Indian Ocean Dipole. *Journal of Geophysical Research*, *115*, C11026. https://doi.org/10.1029/2010JC006423

Nagura, M., & McPhaden, M. J. (2010b). Wyrtki jet dynamics: Seasonal variability. *Journal of Geophysical Research*, *115*, C07009. https://doi.org/10.1029/2009JC005922

Nieves, V., Willis, J. K., & Patzert, W. C. (2015). Recent hiatus caused by decadal shift in Indo-Pacific heating. *Science*, *349*(6247), 532–535. https://doi.org/10.1126/science.aaa4521

Potemra, J. T., & Lukas, R. (1999). Seasonal to interannual modes of sea level variability in the western Pacific and eastern Indian oceans. *Geophysical Research Letters*, *26*(3), 365–368.

Potemra, J. T., & Schneider, N. (2007). Interannual variations of the Indonesian Throughflow. *Journal of Geophysical Research*, *112*, C05035. https://doi.org/10.1029/2006JC003808

Pujiana, K., Gordon, A. L., & Sprintall, J. (2013). Intraseasonal Kelvin wave in Makassar Strait. *Journal of Geophysical Research: Oceans*, *118*, 2023–2034. https://doi.org/10.1002/jgrc.20069

Pujiana, K., Gordon, A. L., Sprintall, J., & Susanto, R. D. (2009). Intraseasonal variability in the Makassar Strait thermocline. *Journal of Marine Research*, *67*(6), 757–777.

Reynolds, R. W., Smith, T. M., Liu, C., Chelton, D. B., Casey, K. S., & Schlax, M. G. (2007). Daily high-resolution-blended analyses for sea surface temperature. *Journal of Climate*, *20*(22), 5473–5496.

Saji, N. H., & Yamagata, T. (2003). Possible impacts of Indian Ocean Dipole mode events on global climate. *Climate Research*, *25*(2), 151–169. https://doi.org/10.3354/cr025151

Santoso, A., Cai, W., England, M. H., & Phipps, S. J. (2011). The role of the Indonesian Throughflow on ENSO dynamics in a coupled climate model. *Journal of Climate*, *24*(3), 585–601. https://doi.org/10.1175/2010jcli3745.1

Schott, F. A., Xie, S.-P., & McCreary, J. P. (2009). Indian ocean circulation and climate variability. *Reviews of Geophysics*, *47*, RG1002. https://doi.org/10.1029/2007RG000245

Shinoda, T., Han, W., Metzger, E. J., & Hurlburt, H. E. (2012). Seasonal variation of the Indonesian Throughflow in Makassar Strait. *Journal of Physical Oceanography*, *42*(7), 1099–1123.

Sprintall, J., Gordon, A. L., Koch-Larrouy, A., Lee, T., Potemra, J. T., Pujiana, K., & Wijffels, S. E. (2014). The Indonesian seas and their role in the coupled ocean-climate system. *Nature Geoscience*, *7*(7), 487–492.

Sprintall, J., Gordon, A. L., Murtugudde, R., & Susanto, R. D. (2000). A semiannual Indian Ocean forced Kelvin wave observed in the Indonesian seas in May 1997. *Journal of Geophysical Research*, *105*(C7), 17217–17230.

Sprintall, J., & Revelard, A. (2014). The Indonesian Throughflow response to Indo-Pacific climate variability. *Journal of Geophysical Research: Oceans*, *119*, 1161–1175. https://doi.org/10.1002/2013jc009533

Susanto, R. D., Ffield, A., Gordon, A. L., & Adi, T. R. (2012). Variability of Indonesian Throughflow within Makassar Strait, 2004–2009. *Journal of Geophysical Research*, *117*, C09013. https://doi.org/10.1029/2012JC008096

Thompson, B., Gnanaseelan, C., & Salvekar, P. S. (2006). Variability in the Indian Ocean circulation and salinity and its impact on SST anomalies during dipole events. *Journal of Marine Research*, *64*, 853–880. https://doi.org/10.1357/002224006779698350

Wijffels, S., & Meyers, G. (2004). An intersection of oceanic waveguides: Variability in the Indonesian Throughflow region. *Journal of Physical Oceanography*, *34*(5), 1232–1253.

Wyrtki, K. (1987). Indonesian through-flow and the associated pressure-gradient. *Journal of Geophysical Research*, *92*(C12), 12941–12946.

Yan, D., Kai, L., Wei, Z., & Wei-Dong, Y. (2012). The Kelvin wave processes in the equatorial Indian Ocean during the 2006–2008 IOD events. *Atmospheric and Oceanic Science Letters*, *5*(4), 324–328.

Yuan, D. L., Zhou, H., & Zhao, X. (2013). Interannual climate variability over the tropical Pacific ocean induced by the Indian Ocean dipole through the Indonesian Throughflow. *Journal of Climate*, *26*(9), 2845–2861.